OXFORD

SOT | Society of Toxicology
www.toxsci.oxfordjournals.org

TOXICOLOGICAL SCIENCES, 150(2), 2016, 418–428

doi: 10.1093/toxsci/kfw005
Advance Access Publication Date: January 14, 2016
Research Article

Toxicological Assessment of CoO and La_2O_3 Metal Oxide Nanoparticles in Human Small Airway Epithelial Cells

Jennifer D. Sisler,* Sandra V. Pirela,† Justine Shaffer,* Amy L. Mihalchik,* William P. Chisholm,* Michael E. Andrew,* Diane Schwegler-Berry,* Vincent Castranova,‡ Philip Demokritou,† and Yong Qian*,[1]

*Health Effects Laboratory Division, National Institute for Occupational Safety and Health, Morgantown, West Virginia 26505; †T.H. Chan School of Public Health, Harvard University, Boston, Massachusetts 02115; and ‡Department of Pharmaceutical Sciences, West Virginia University, Morgantown, West Virginia 26505

Disclaimer: The findings and conclusions in this report are of the authors and do not necessarily represent the views of the National Institute for Occupational Safety and Health.

[1]To whom correspondence should be addressed at Health Effects Laboratory Division, NIOSH, 1095 Willowdale Road, Morgantown, WV 26505. Fax: (304) 285-5938. E-mail: yaq2@cdc.gov.

ABSTRACT

Cobalt monoxide (CoO) and lanthanum oxide (La_2O_3) nanoparticles are 2 metal oxide nanoparticles with different redox potentials according to their semiconductor properties. By utilizing these two nanoparticles, this study sought to determine how metal oxide nanoparticle's mode of toxicological action is related to their physio-chemical properties in human small airway epithelial cells (SAEC). We investigated cellular toxicity, production of superoxide radicals and alterations in gene expression related to oxidative stress, and cellular death at 6 and 24 h following exposure to CoO and La_2O_3 (administered doses: 0, 5, 25, and 50 μg/ml) nanoparticles. CoO nanoparticles induced gene expression related to oxidative stress at 6 h. After characterizing the nanoparticles, transmission electron microscope analysis showed SAEC engulfed CoO and La_2O_3 nanoparticles. CoO nanoparticles were toxic after 6 and 24 h of exposure to 25.0 and 50.0 μg/ml administered doses, whereas, La_2O_3 nanoparticles were toxic only after 24 h using the same administered doses. Based upon the Volumetric Centrifugation Method *in vivo* Sedimentation, Diffusion, and Dosimetry, the dose of CoO and La_2O_3 nanoparticles delivered at 6 and 24 h were determined to be: CoO: 1.25, 6.25, and 12.5 μg/ml; La_2O_3: 5, 25, and 50 μg/ml and CoO: 4, 20, and 40 μg/ml; and La_2O_3: 5, 25, 50 μg/ml, respectively. CoO nanoparticles produced more superoxide radicals and caused greater stimulation of total tyrosine and threonine phosphorylation at both 6 and 24 h when compared with La_2O_3 nanoparticles. Taken together, these data provide evidence that different toxicological modes of action were involved in CoO and La_2O_3 metal oxide nanoparticle-induced cellular toxicity.

Key words: nanoparticles; metal oxides; cytotoxicity; cell culture; oxidative stress.

It has been hypothesized that the toxicity of a nanomaterial is largely due to their physicochemical properties, such as: size, morphology, oxidant generation, surface functionalization, and rate of dissolution (Castranova 2011; Sarkar *et al.*, 2014). The specific properties of a nanomaterial allow them to cross the cell membrane both *in vitro* and *in vivo* leading to the alteration of cell physiology, resulting in cytotoxicity (Castranova 2011; Cohen *et al.*, 2014a; Jeng and Swanson, 2006; Katsnelson *et al.*, 2015; Konduru *et al.*, 2014; Nel *et al.*, 2006; Roy *et al.*, 2014; Zhou *et al.*, 2014). Metal oxide nanoparticles are unique in their

catalytic activities for redox reactions, which are correlated to their abilities to induce oxygen radicals (Nel *et al.*, 2006). Moreover, published data have shown that metal oxide nanoparticles have the ability to induce the production of reactive oxygen species (ROS) and affect the expression of antioxidant protein and enzymes of the defense systems both *in vitro* and *in vivo* resulting in oxidative stress. Oxidative stress can lead to cytotoxicity, inflammation, and fibrosis both *in vitro* and *in vivo* (Schrand *et al.*, 2010; Xie *et al.*, 2011; Zhang *et al.*, 2012).

Other unique properties of metal oxide nanoparticles are their mechanical, electrical, and optical properties. Some metal oxide nanomaterials have the ability to be a semiconducting material and can serve as conduits for electron transfer between aqueous reactants. Studies have shown that these semiconducting properties may be responsible for generating adverse health effects (Antonini *et al.*, 1996; McNeilly *et al.*, 2004). The electrons transferred between metal oxide nanoparticles and aqueous reactants depend on similarities in the energetic states of both the metal oxide nanoparticles and the ambient redox-active aqueous substances (Nel *et al.*, 2006). Through the evaluation of metal oxide nanoparticles, Dr. Nel's group predicted that if the conduction band energy overlapped with that of the redox potential of the cell, then the metal oxide nanoparticle would produce superoxide radicals and cause cytotoxicity (Kaweeteerawat *et al.*, 2015; Zhang *et al.*, 2012). The relevant energy levels for metal oxide nanoparticles are from the top of the valence band (Ev) to the bottom of the conduction band (Ec). The relevant energy level for aqueous substances is their standard redox potential (E^0) (Nel *et al.*, 2006; Zhang *et al.*, 2012). The relative energetics of Ev or Ec versus E^0 would determine the feasibility of electrons to be transferred between the semiconductor and redox-active bystanders (Nel *et al.*, 2006; Zhang *et al.*, 2012). The permissive electron transfer between the particle surfaces and the cellular redox couples would occur if an overlap exists between Ec and E^0, which would lead to formation of oxidizing or reducing substances that decrease antioxidant levels, increase production of ROS and/or oxidized biological materials (Burello and Worth, 2011a,b). In contrast, if an energetic band gap exists between Ev and Ec versus E^0, no permissive electron transfer could occur, and consequently, less oxidative stress would be induced. Dr. Nel's group investigated 24 metal oxide nanoparticles for their toxicological potential according to their conduction band energy levels. Among them, Cobalt monoxide (CoO) nanoparticles have a potential overlap of Ec with the cellular redox interval and are therefore predicted to have electrons transferred between CoO nanoparticles and cellular redox couples to induce oxygen radicals and oxidative stress, leading to cellular toxicity. On the contrary, lanthanum oxide (La_2O_3) nanoparticles do not have a potential overlap of Ec with cellular redox interval and thus are predicted to be weak in inducing of oxygen radicals and oxidative stress. Indeed, their whole animal and cellular studies showed that a correlation exists between their redox-related toxicity and conduction band energy (Zhang *et al.*, 2012). Therefore, the toxicological mode of action between CoO nanoparticles and La_2O_3 nanoparticles could be fundamentally different.

The cytotoxicity of CoO nanoparticles has been demonstrated in a number of physiological relevant *in vitro* models. CoO nanoparticles were considered to be cytotoxic in human lymphocytes by inducing ROS, by the dissolution of Co^{++} from CoO nanoparticles (Chattopadhyay *et al.*, 2015). Chattopadhyay *et al.* also showed that CoO nanoparticles in *vivo* are cytotoxic through inducing oxidative stress (Chattopadhyay *et al.*, 2015). A gene expression study showed that CoO nanoparticles have the ability to induce inflammation and cytotoxicity in alveolar A549 and bronchial BEAS-2B epithelial cells (Verstraelen *et al.*, 2014); however, the gene expression profile is different between the two *in vitro* lung epithelial cell lines suggesting the signaling cascades to cause an inflammatory response and cytotoxicity could be slightly different. Others have looked at the cytotoxicity of La_2O_3 nanoparticles within RAW264.7 cells and A549 cells and determined that with increasing amounts of La_2O_3 nanoparticles and increased incubation time, La_2O_3 nanoparticles become more cytotoxic and that the size of the La_2O_3 particles plays a large role in cytotoxicity (Lim, 2015).

This study sought to determine how the mode of toxicological action is related to physio-chemical properties of nanoparticles. CoO and La_2O_3 nanoparticles were analyzed to compare their bioactivity and toxicity in human small airway epithelial cells (SAEC), as well as, the cellular ROS levels induced following exposure. Furthermore, we determined whether different molecular signaling were involved in CoO and La_2O_3 nanoparticle-induced toxicity.

MATERIALS AND METHODS

Source and characterization of metal oxide nanoparticles

The CoO nanoparticles were purchased from SkySpring Nanomaterials (Houston, Texas) (Catalogue Number: 2310SC) and La_2O_3 nanoparticles were purchased from Nanostructured & Amorphous Materials, Inc (Houston, Texas) (Catalog Number: 2920RE).

Specific surface areas of CoO and La_2O_3 nanoparticles determined by the Brunauer–Emmett–Teller method (Quantachrome, Boynton Beach, Florida) were 18.34 and 6.87 m^2/g, respectively. The equivalent primary particle diameter of each metal oxide was subsequently estimated by transmission electron microscopy (TEM) to be 53.55 nm for CoO nanoparticles and 134.22 nm for La_2O_3 nanoparticles. TEM images of the CoO and La_2O_3 nanoparticle powder can be found in Supplementary Figure 1.

CoO and La_2O_3 nanoparticles suspension preparation and characterization

Particle dispersions were prepared following a previously published protocol (Ametamey *et al.*, 1996; Cohen *et al.*, 2013). In summary, the powders were suspended in dispersion media (DM) containing: 0.6 mg/ml bovine serum albumin (BSA), 100 μg/ml DPPC, 0.55M Glucose in phosphate-buffered saline and sonicated to their determined critical delivered sonication energy (CoO nanoparticles: 268 J/ml, La_2O_3 nanoparticles: 371.85 J/ml). Subsequently, the particle suspensions were diluted in SAEC basal culture medium (SABM) and characterized for intensity-weighted hydrodynamic diameter (d_H), polydispersity index (PdI), zeta potential (ζ), and specific conductance (σ) by dynamic light scattering (DLS) following the protocol described in Cohen *et al.*, 2013. The effective density (ρ_{agg}) of the formed agglomerates, which plays an important role in the settling and dosimetry *in vitro*, was also measured using the recently developed Volumetric Centrifugation Method (VCM) (DeLoid *et al.*, 2014).

Dosimetric considerations for *in vitro* testing

The conversion of the administered and delivered *in vitro* doses was done following the hybrid VCM-*in vivo* Sedimentation, Diffusion and Dosimetry (VCM-ISDD) dosimetry methodology recently published by the authors (Cohen *et al.*, 2014b; DeLoid

et al., 2014; Pal et al., 2015). This 2-step integrated dosimetric approach enables the calculation of the fraction of administered particles deposited on the cells (f_D) in a standard 6- and 96-well plate as a function of *in vitro* exposure duration. Subsequently, the average hydrodynamic diameter, d_H, measured by DLS, and the VCM-measured effective density (DeLoid et al., 2014) of the formed agglomerate were used as input to the VCM-ISDD fate and transport numerical model to calculate the f_D as a function of the 24-h exposure duration. Further, to allow for the accurate estimation of the delivered to cell dose metrics (mass, particle number, total surface) as a function of time, the Relevant *in vitro* Dosimetry (RID) functions were calculated for both particle suspension in a 6- and 96-well plate experimental condition as described in Cohen et al. (2014b). In brief, the RID functions were derived from the total mass administered (M), total surface area dose (SA), and total particle number dose (N) by using the equations 1 through 3, as follows:

1. $M = \gamma \times V$; where M (μg) is the total mass dose, V is the volume of exposure media (ml) applied directly to the cells in culture and γ (μg/ml) is the mass concentration of the ENM suspension.
2. $N = \frac{M}{\left(\frac{4}{3}\pi r_H^3\right)\times\rho_E}$; where N (#) is the total particle number dose, r_H (cm) is the hydrodynamic radius, and ρ_E, (g/cm^3) is the agglomerate effective density.
3. $SA = \left(4\pi r_H^2\right) \times N$: where SA (cm^2) is the total surface area dose.

Once these three metrics have been calculated, the RID functions for delivered dose metrics can now be computed using equations 4 through 6 and using as input the material-media specific parameters obtained from the fate and transport algorithm (α, deposition constant and t, exposure duration), as follows:

4. Delivered to cell mass (RID_M, μg): $RID_M = (1 - e^{-\alpha t}) \times M$
5. Delivered to cell particle number (RID_N, number of particles): $RID_N = (1 - e^{-\alpha t}) \times N$
6. Delivered to cell surface area (RID_{SA}, cm^2): $RID_{SA} = (1 - e^{-\alpha t}) \times SA$

Cell culture

SAEC were a gift from by Dr Tom K. Hei at Columbia University (New York) and were maintained as previously described (Piao et al., 2005). The SAEC were maintained in serum free SABM with the following supplemental growth factors (Bovine Pituitary Extract, Hydrocortisone, Human Epidermal Growth Factor, Epinephrine, Transferrin, Insulin, Retinoic, Triiodothyronine, Gentimicin Amphoteracin-B, and BSA-fatty acid free) provided by the manufacturer (Lonza Inc., Allendale, New Jersey). For each experiment, SAEC were plated at the appropriate density and allowed to fully attach for 24 h, after which the medium was changed to dispose of dead cells. After 48 h, the SAEC were given SABM media free of the supplemental growth factors for 24 h and treated with DM, CoO, or La_2O_3 nanoparticles for either 6 or 24 h.

Transmission electron microscopy

After SAEC were dosed with CoO or La_2O_3 nanoparticles at 0.0, 5.0, 25, or 50 μg/ml for either 6 or 24 h, the cells were trypsinized and centrifuged at 1500 $\times$ g for 5 min at room temperature and then fixed with Karnovsky's fixative (2.5% glutaldehyde, 2.5% paraformaldehyde in 0.1 M Sodium Cacodylic buffer). The samples were postfixed in osmium tetroxide, mordanted in 1% tannic acid and stained in bloc in 0.5% uranyl acetate, embedded in epon, sectioned, and stained with Reynold's lead citrate and uranyl acetate. Sections were imaged with the JEOL 1220 transmission electron microscope (Tokyo, Japan).

Cytotoxicity of CoO and La_2O_3 nanoparticles

SAEC were plated in a 96-well plate at a density of 1.5 $\times$ 10^4 cells per well (BD Biosciences, New Jersey). To determine the changes in cellular proliferation after treatment with CoO or La_2O_3 nanoparticles, the Cell Titer 96 Aqueous One Solution Cell Proliferation Assay kit (Promega, Wisconsin) was used, following manufacturer's guidelines. The following concentrations of CoO and La_2O_3 nanoparticles were used to determine the cytotoxicity in the (3-(4,5-dimethylthizaol-2-yl)-5-(3-carboxymethoxyphenyl)-2-(4-sulfophenyl)-2H-tetrazolium (MTS) assay at 6 or 24 h: 0.0, 5.0, 25, and 50 μg/ml.

ROS produced by CoO and La_2O_3 nanoparticles

In a 96-well plate, SAEC were plated at 1.5 $\times$ 10^4 cells per well (BD Biosciences). For the last 30 min of the 6 or 24 h treatment with DM, CoO or La_2O_3 nanoparticles, 5 μM 2′,7′-dichlorofluorescin diacetate (DCFDA) (Invitrogen, New York) in DMSO was added, then the plate was read at 492 and 517 nm in a plate reader.

Western blots

Whole cell extracts were gathered from SAEC treated with CoO or La_2O_3 nanoparticles at 0.0, 5.0, 25, or 50 μg/ml using RIPA buffer (150 mM NaCl, 10 mM Tris pH 7.4, 2 mM EDTA, 1% IGEPAL, 1% sodium deoxycholate, 0.1% sodium dodecyl sulfate) with the addition of 10 μg/ml protease inhibitor cocktail and 10 μg/ml phosphatase inhibitor (Thermo Fisher Scientific, Pittsburgh, Pennsylvania). Protein concentration was determined using a BCA protein assay kit (Thermo Fisher Scientific). 15 μg of protein was run on an sodium dodecyl sulfate polyacrylamide gel electrophoresis (SDS–PAGE) gel, transferred onto Polyvinylidene fluoride (PVDF) membrane, and blocked with 5% BSA. The membranes were probed with total phospho-tyrosine antibody, total phospho-threonine antibody, HIF-1α antibody (Cell Signaling Technology, Boston, Massachusetts), or beta actin antibody (Sigma Aldrich, St. Louis, Missouri) as an internal control. Membranes were washed with TBS-T (62.5 mM Tris pH 7.4, 150 mM NaCl, 0.05% Tween 20) three times and incubated with a secondary antibody. Membranes were developed using ECL (Thermo Fisher Scientific).

Gene expression analysis

RNA was extracted from SAEC dosed with CoO or La_2O_3 nanoparticles at 0.0, 5.0, 25, or 50 μg/ml for 6 or 24 h using Tri Reagent (Thermo Fisher Scientific) according to manufacturer's guidelines. RNA concentrations were determined using a NanoDrop 1000 Spectrophotometer (NanoDrop Tech, Germany). Next, 1 μg of protein was used to generate cDNA according to manufacturer guidelines in the High Capacity cDNA Reverse Transcription Kit (Life Technologies, Grand Island, New York). The cDNA was then used to analyze gene expression using TaqMan Universal PCR Master Mix (Life Technologies) according to instructions provided by the manufacturer along with the TaqMan Primers (Life Technologies) listed in Supplementary Table 1 using the 7500 Real-time PCR System (Life Technologies). The following genes were analyzed: B-cell

TABLE 1. Properties of CoO and La_2O_3 Nanoparticles in SABM

Material	Media	d_H (nm)	PdI	ζ (mV)	Σ (mS/cm)	ρ_{agg} (g/cm^3)
CoO	SABM	263.8 ± 2.237	0.326 ± 0.041	−9.95 ± 0.827	15.2 ±0.814	1.55 ± 0.043
La_2O_3	SABM	1591 ± 262.3	0.348 ± 0.087	−48.8 ± 16.1	1260 ± 203	1.20 ± 0.009

d_H: hydrodynamic diameter, PdI: polydispersity index; ζ: zeta potential, σ: specific conductance; ρ_{agg}: effective density. Values represent the mean (± SD) of a triplicate reading.

lymphoma 2 (BCL_2), tumor protein p53 (p53), hypoxia-inducible factor 1-alpha (Hif1α), metallothionein 3 (MT3), nitric oxide synthase 1 (NOS1), nitric oxide synthase 2 (NOS2), prostaglandin-endoperoside synthase 2 (PTGS2 (Cox2)), superoxide dismutase 1 (SOD1), superoxide dismutase 2 (SOD2), superoxide dismutase 3 (SOD3), and throredoxin reductase 1 (TXNRD1). Beta actin was used as the internal control. Relative gene expression was analyzed using the $2^{-\Delta\Delta CT}$ method.

Statistical analysis

Statistical comparisons for the SAEC response to exposure to CoO and La_2O_3 nanoparticles, separately and across three concentrations including DM controls were performed separately for each of two exposure times (6 or 24 h) using analysis of variance. Since variance estimates were different across treatment groups, the ANOVA models were estimated using an unequal variance method available from SAS PROC MIXED (Littell *et al.*, 2002). Similarly, comparisons across exposure times for each concentration (0, 5, 25, or 50 μg/ml) were performed using unequal variance ANOVA. All statistical tests were 2-tailed with significance level equal or less than 0.05.

RESULTS

Nanoparticle Dispersion Characterization in SABM

Table 1 summarizes the particle colloidal properties in the biological media used in the study, including the DLS-measured hydrodynamic diameter (d_H), zeta potential (ζ), polydispersity index (PdI), and specific conductance (σ). The CoO nanoparticle suspension exhibited a d_H in SABM of 263.8 nm, whereas La_2O_3 nanoparticles were determined to have a d_H of 1591 nm when dispersed in SABM. The PdI values for both suspensions were approximately 0.3, which reflects a distribution of monodispersed particles. Observed values of zeta potential were strongly negative for both particles suspended in cellular media, with negative values as high −9.95 and −48.8 mV for CoO and La_2O_3 nanoparticles, respectively.

Additionally, the VCM-measured effective density of CoO nanoparticles was 1.55 g/cm^3, whereas that of the La_2O_3 nanoparticles was 1.20 g/cm^3 when suspended in SABM media (Table 1). It is worth noting that both the effective density and hydrodynamic diameter (Cohen *et al.*, 2013; DeLoid *et al.*, 2014, No. 430) of formed agglomerates are important determinants of fate and transport in the *in vitro* system and define settling rates and dosimetry *in vitro*.

Dosimetric Considerations for *in vitro* Testing

The delivered cell dose at a given exposure time point may not always be the same as the dose administered (Cohen *et al.*, 2013). The settling rate of the formed agglomerates *in vitro* is defined by two fundamental parameters, the hydrodynamic diameter of the formed agglomerate and their effective density (Cohen *et al.*, 2013; DeLoid *et al.*, 2014). Using the recently developed Harvard *in vitro* dosimetry methodology (Cohen *et al.*, 2014b), the fraction of the administered particles that deposit on the cells located at the bottom of the treatment well as a function of time was calculated and presented in Figure 1. The deposition fraction constant (α) as well as the number of hours it will take for 90% of the administered dose to deposit (t_{90}) for both particle suspensions is presented in Table 2. The La_2O_3 nanoparticles settled significantly faster than CoO nanoparticles when suspended in SABM. More specifically, it took less than 3 h for all of the administered La_2O_3 nanoparticle mass to deposit on the cells while approximately 80% of administered CoO nanoparticles reached the bottom of the well in 24 h. Table 3 shows the RID functions for both particles suspended in media both in a 6- and 96-well plate. It is worth noting that other dose metrics beyond delivered mass such as delivered surface and particle number, respectively defined by the RID_N and RID_{SA} might better describe the dose response relationships observed here (Oberdorster *et al.*, 2007). Indeed, the RID_N and RID_{SA} for CoO nanoparticles are larger than that for the La_2O_3 nanoparticles. As mentioned in the Materials and Methods section of the manuscript, the d_H and the effective density of the particle-media agglomerate have an effect on the fate and transport of the particles, consequently affecting dosimetry considerations *in vitro* (ie, RID functions). It is a possible that a larger number of CoO particles in addition to a larger CoO nanoparticle surface area allows for more interaction to occur between the CoO particles and the treated cells. Thus, increasing the adverse response exhibited by the CoO-treated cells when compared with the La_2O_3-treated cells.

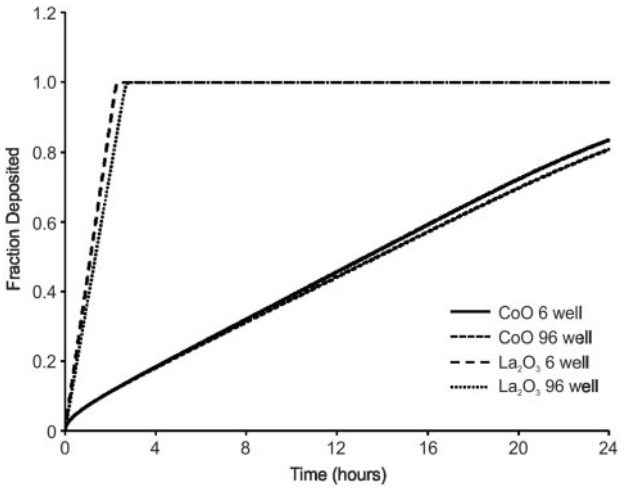

FIG. 1. Fraction deposited of cobalt monoxide (CoO) nanoparticles and lanthanum oxide (La_2O_3) nanoparticles as a function of time. Fractions deposited were calculated using the estimated effective density. Plots are presented for the nanoparticles suspeSnded in SABM. The f_D for CoO nanoparticles is 0.8 and La_2O_3 nanoparticles is 1.0 for a 24-h *in vitro* exposure duration in both a 6- and 96-well exposure condition.

TABLE 2. Delivered Dose Metrics for CoO and La_2O_3 Nanoparticle Suspensions in SABM

Material	6-Well Plate		96-Well Plate	
	α (h^{-1})	t_{90} (h)	α (h^{-1})	t_{90} (h)
CoO	0.0546	42.18	0.0521	44.18
La_2O_3	0.910	2.53	0.7672	3.00

α (h^{-1}): deposition fraction constant; t_{90} (h): time for delivery of 90% of administered dose (h).

TABLE 3. RID Functions for CoO and La_2O_3 Nanoparticle Suspensions in SABM for an Exposure Duration of 24 h and an Administered Dose of 50.0 μg/ml

	6-Well Plate		96-Well Plate	
Material	CoO	La_2O_3	CoO	La_2O_3
RID_M (μg)	52.58	150	3.57	5.00
RID_N (number of particles)	3.52×10^{15}	5.94×10^{13}	2.39×10^{14}	1.98×10^{12}
RID_{SA} (cm^2)	7.70×10^{6}	4.72×10^{6}	5.52×10^{5}	1.57×10^{5}

Engulfment of CoO and La_2O_3 Nanoparticles by SAEC

Within this study, it was of importance to determine if SAEC engulfed the nanomaterial. To determine this, SAEC were analyzed using TEM after being treated with either CoO or La_2O_3 nanoparticles at 0.0, 5.0, 25.0, 50.0 μg/ml at both 6 and 24 h. Figure 2 demonstrates that CoO and La_2O_3 nanoparticles were taken up by SAEC at each dose tested, as seen by the arrows.

Cytotoxicity of CoO and La_2O_3 Nanoparticles

It has been demonstrated that metal oxides nanoparticles are toxic (Jeng and Swanson, 2006; Schrand *et al.*, 2010). To determine the degree of toxicity of CoO and La_2O_3 nanoparticles in SAEC, we measured cytotoxicity using an MTS Assay after treatment with CoO or La_2O_3 nanoparticles at 0.0, 5.0, 25.0, or 50.0 μg/ml for 6 or 24 h. As seen in Figure 3A, CoO nanoparticles decreased cell viability as the doses increased at both 6 and 24 h. However, La_2O_3 nanoparticles were only toxic in a dose dependent manner after a 24 h exposure. There was no significant toxicity observed after 6 h of treatment with La_2O_3 at 5.0, 25.0 or 50 μg/ml. When comparing the toxicity of CoO nanoparticles to that of La_2O_3 nanoparticles, CoO nanoparticles were significantly more toxic both at 25 and 50 μg/ml after 6 h of treatment and at 25 μg/ml after 24 h of treatment. There were no changes in toxicity at 5 μg/ml after 6 or 24 h treatment of CoO or La_2O_3 nanoparticles. Taken together, these data suggest that CoO nanoparticles are more toxic than La_2O_3 nanoparticles in SAEC after 6 and 24 h treatment. As seen in Figures 3B and 3C of the slope of each material's dose response graph (−1.7351 for CoO and −0.9018 for La_2O_3), it can be observed that CoO nanoparticles appears to be more toxic than La_2O_3 nanoparticles in SAEC for the range of delivered mass doses. Particularly, at the same delivered doses of 2.5 μg/ml after 24 h treatment, it is evident that metabolic activity drops 7 times more after treatment with CoO nanoparticles (23.1%) than with La_2O_3 nanoparticles (3.3%). It is worth noting that the size is one of the factors that define the settling rate and the delivered to cell dose as a function of exposure time. Based on the dosimetric analysis performed here, it is clear that La_2O_3 nanoparticles had a higher delivered dose compared to that of CoO nanoparticles. Despite of the fact that La_2O_3 nanoparticles settled faster than the CoO nanoparticles, the percent viability following treatment with CoO decreased at a much higher rate than in cells treated with La_2O_3 nanoparticles, which is indicative of the higher biological reactivity of the CoO nanoparticles.

Production of ROS By CoO and La_2O_3 Nanoparticles

The production of ROS by metal oxide nanoparticles has been well established both *in vivo* and *in vitro*, and has been shown to play a key role altering cellular signaling cascades (Sarkar *et al.*, 2014; Zhang *et al.*, 2012). To determine if either CoO or La_2O_3 nanoparticles produce ROS, SAEC were treated for 6 or 24 h at 0.0, 5.0, 25, or 50 μg/ml of either CoO or La_2O_3 nanoparticles and then treated with 5 μM DCFDA for the last 30 min of exposure. DCFDA in the presence of free radicals is oxidized and cleaved of the acetate group to become DCF, which produces fluorescence. As seen in Figure 4, cells treated with 25 or 50 μg/ml of CoO nanoparticles induced more fluorescence in comparison to La_2O_3 nanoparticles treated cells at both 6 and 24 h, indicating that CoO nanoparticles produce more ROS. However, there was no significant induction of fluorescence in cells treated with 5.0 μg/ml of either CoO or La_2O_3 nanoparticles. Moreover, CoO nanoparticles also showed a trend of increased super oxide production at increasing doses of nanoparticles; however, this observation was not seen in cells treated with La_2O_3 nanoparticles at either exposure duration. These data suggest that the CoO nanoparticles produce more ROS when compared with La_2O_3 nanoparticles at both 25 and 50 μg/ml after both 6 and 24 h.

Increase in Total Tyrosine and Threonine Phosphorylation

Tyrosine and threonine phosphorylation of proteins is a key step in the activation of cellular signaling pathways (Hunter, 1995; Marshall, 1995). Changes in either tyrosine or threonine phosphorylation due to nanoparticle exposure can alter the cellular bioactivity on a global scale. Whole cell lysates were taken from SAEC treated with either CoO or La_2O_3 nanoparticles for 6 or 24 h at 0.0 5.0, 25.0, or 50.0 μg/ml. As can be seen in Figure 5, there was increased total tyrosine phosphorylation at all doses of CoO nanoparticles at 6 and 24 h compared with La_2O_3 nanoparticle treated SAEC. There were also increases seen with total threonine phosphorylation at 6 h for CoO nanoparticle-treated cells; however, threonine was further induced after a 24 h treatment with CoO. There were increases seen at 24 h of total threnonine phosphorylation of cells treated with La_2O_3 nanoparticles; however, induction was not as great as that for cells treated with CoO nanoparticles. Taken together, these data suggest that the CoO nanoparticles are more bioactive than the La_2O_3 nanoparticles, causing greater changes in total tyrosine and threonine phosphorylation at a both 6 and 24 h at the various doses studied.

Alteration in Gene Expression in SAEC Due to CoO and La_2O_3 Nanoparticles

Given the changes seen in total tyrosine and threonine phosphorylation in SAEC treated with either CoO or La_2O_3 nanoparticles, it was of interest to determine if this translated into alterations in gene expression. To determine this, RNA was isolated from SAEC dosed for 6 or 24 h at 0.0, 5.0, 25.0, and 50.0 μg/ml with either CoO or La_2O_3 nanoparticles and then analyzed

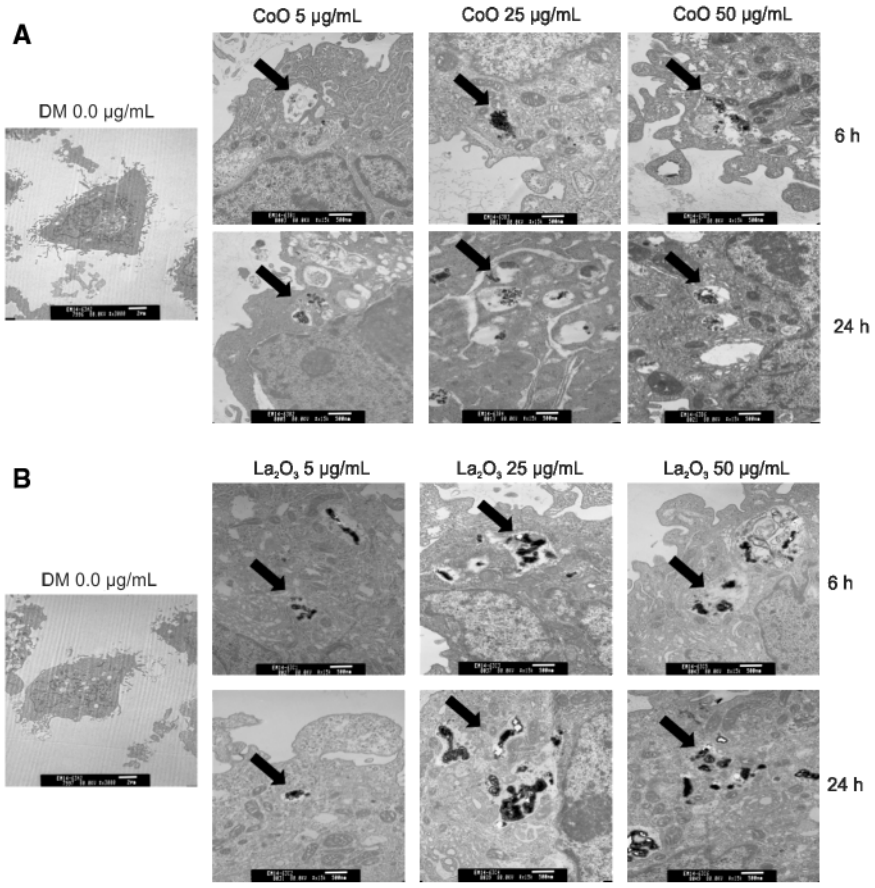

FIG. 2. SAEC engulf CoO and La_2O_3 nanoparticles. SAEC were treated for either 6 or 24 h with (A) CoO or (B) La_2O_3 nanoparticles at 0.0, 5.0, 25.0, or 50.0 ug/ml administered dose. SAEC were then fixed with Karnovsky's fixative, stained with osmium and imaged with a transmission electron microscope. Particles are identified with arrows. Images represent n = 3.

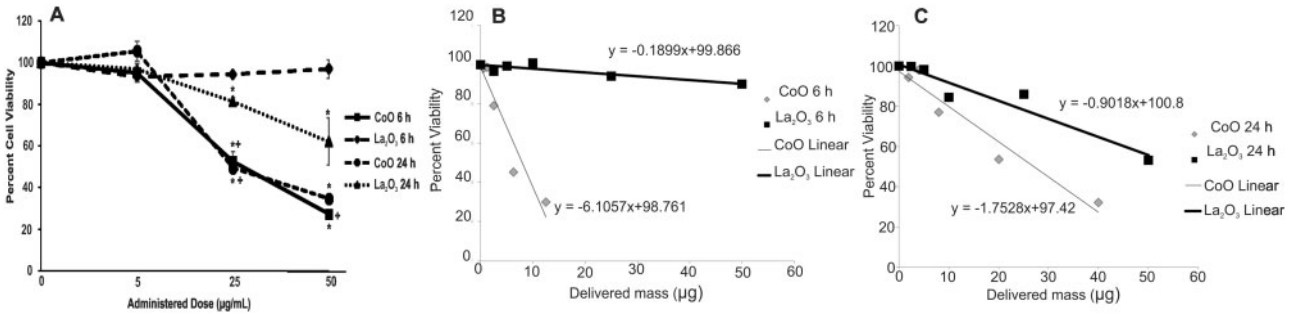

FIG. 3. Cytotoxicity of CoO and La_2O_3 nanoparticles. SAEC were treated with 0.0 5.0, 25.0, or 50.0 μg/ml administered dose of CoO or La_2O_3 nanoparticles for 6 or 24 h. A, The cells were then assayed using an MTS assay. Delivered mass of CoO and La_2O_3 nanoparticles at (B) 6 h and (C) 24 h and the respective linear fit line. The slope of the fit line is used in determining the change in percent viability per unit of delivered mass specific to each nanoparticle treatment. Values represent the percent cell viability with n = 3, * indicates $P < .05$ compared to 0.0 μg/ml control. + indicates $P < .05$ compared to La_2O_3 at same time point.

for alterations in gene expression relating to either apoptosis or oxidative stress (ATK1, BCL2, p53, Hif1α, MT3, NOS1, NOS2, PTGS2 (COX2), SOD1, SOD2, SOD3, and TXNRD1). While there were changes seen within the gene expression that related to a dose response to either CoO or La_2O_3 nanoparticles, the data in Figure 6 are only the genes that showed a significant differences between CoO and La_2O_3 nanoparticle treated cells at 6 h. As can be seen in Figure 6, CoO nanoparticles had significantly elevated gene expression of PTGS2(COX2), SOD3, and MT3 at either 25 or 50 μg/ml after 6 h compared with La_2O_3-treated SAEC. The gene expression of NOS2 is decreased compared with the DM CTRL at both 25 and 50 μg/ml for both nanoparticles assayed; however, NOS2 expression is further decreased at 50 μg/ml in cells treated with La_2O_3 nanoparticles when comparing to cells treated with CoO nanoparticles. There were no significant changes seen between cells treated with either CoO or La_2O_3 nanoparticles at the various exposure doses at 6 or 24 h in expression of AKT1, BCL2, p53, HIf1α, SOD1, SOD2, or TXNRD1 (data not shown). After 24 h post exposure, there were no significantly changes observed in the gene expressions (data not shown). There were also no significant changes seen in SAEC-treated cells at 5 μg/ml of either CoO or La_2O_3 nanoparticles (data not shown). These

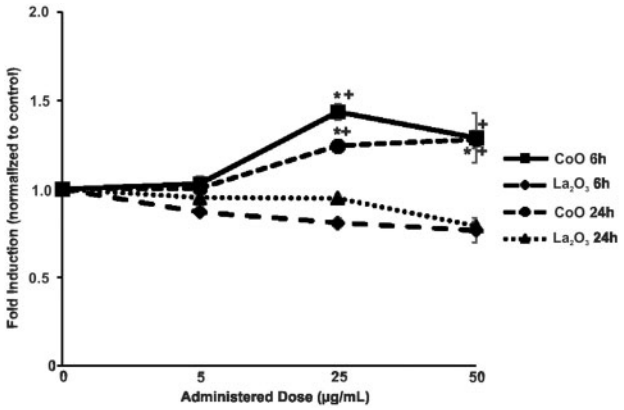

FIG. 4. SAEC Production of ROS by CoO and La_2O_3 nanoparticles. SAEC were treated for 6 or 24 h with CoO or La_2O_3 nanoparticles with the following doses: 0.0, 5.0, 25.0, and 50.0 μg/ml and for the last 30 min 5 μM DCFDA was added to analyze superoxide production. Fluorescence was measured using a plate reader. Values were normalized to 0.0 μg/ml control ± Standard error. n = 3, * indicates $P < .05$ compared to 0.0 μg/ml control. + indicates $P < .05$ compared to La_2O_3 nanoparticles.

data demonstrated that CoO and La_2O_3 nanoparticles induce different gene expression profiles in SAEC, suggesting that they activate different molecular pathways.

Induction of HIF-1α Due to CoO Nanoparticle

To explore the potential cellular mechanisms that could play a key role in CoO and La_2O_3 nanoparticle induced cytotoxicity, HIF-1α protein expression was examined after 6 h treatment of CoO and La_2O_3 nanoparticles in SAEC. HIF-1α gene expression did not show any significant changes when measured; however, the transcription factor is well known to be regulated translationally (Wenger, 2000). As seen in Figure 7, CoO nanoparticles induced HIF-1α expression at all doses analyzed (5, 25 and 50 μg/ml) when compared with DM control and La_2O_3 nanoparticles. No detectable HIF-1α expression was seen in the DM or La_2O_3 nanoparticle samples examined at any dose (5, 25, or 50 μg/ml). Taken together these data indicate that CoO nanoparticles may induce cytotoxicity through the induction of HIF-1α protein expression.

DISCUSSION

CoO nanoparticles are used in a wide variety of applications such as a drying agent for oil paints, varnishes, magnetic toners, and inks. They are fundamentally important for manufacturing rechargeable batteries, magnets and wave shielding for cellular phones. CoO nanoparticles have also been used in propane gas as an oxidizing agent, as well as, a contrasting agent in magnetic resonance imaging (MRI) machines. La_2O_3 nanoparticles have been incorporated and used for the following purposes: high refractive optical fibers, agricultural films, automobile exhaust catalyst, electroforming electrode materials, as an anti-corrosion, to reduce electrode wear, and as a magnet for magnetic storage and within a MRI machine. La_2O_3 nanoparticles are also used within optical glass, for nano-optical conversion efficiency and to chemically improve the burning rate of propellants. Due to the large presence of these particles in various occupations, it is important to study the potential toxicological effects of both La_2O_3 and CoO nanoparticles on the exposed individuals.

The results of this study demonstrate that different toxicological modes of action are involved in CoO and La_2O_3 nanoparticle-induced cell toxicity in SAEC. Furthermore, this study examines the actual delivered mass to SAEC after equal administrated doses. As seen in this study, the delivered doses are not equivalent to the administrated doses and upon using the VCM-ISDD, it was determined that fewer CoO nanoparticles were needed to produce cytotoxicity than La_2O_3 nanoparticles. Within this study, gene expression was examined to determine specific molecular pathways that were activated within SAEC after treatment with CoO and La_2O_3 nanoparticles. Both CoO and La_2O_3 nanoparticles were able to be engulfed by SAEC at the various doses administered. Using the VCM-ISDD, it was determined that a smaller amount of CoO nanoparticles was delivered to the cells at all doses when compared with La_2O_3 delivered mass. However, when comparing cell viability after treatment, CoO nanoparticles were considered more cytotoxic at the same administered dose, indicating that less CoO nanoparticles are needed to cause equivalent amounts of cytotoxicity to that induced by La_2O_3 nanoparticles. SAEC treated with 25.0 and 50.0 μg/ml CoO nanoparticles produced more ROS and were more cytotoxic at both 6 and 24 h in comparison to La_2O_3 nanoparticles. CoO nanoparticles increased the global tyrosine and threonine phosphorylation footprint in SAEC to a higher degree than La_2O_3 nanoparticles. Moreover, several genes related to oxidative stress were induced in SAEC exposed to CoO nanoparticles in comparison to La_2O_3 nanoparticles.

It has been proposed that the evaluation of the physicochemical properties of metal oxide nanoparticles could predict their toxicity. However, a knowledge gap exists regarding the association between the unique physicochemical properties of such metal oxide nanoparticles and their toxicological profile. Several published studies have shown that a difference in the band energy of metal oxide nanoparticles could be used to predict their potential ROS production (Burello and Worth, 2011a,b; Zhang *et al.*, 2012). CoO nanoparticles are known to have an overlapping redox potential with cells, indicative of higher ROS induction potential, while La_2O_3 nanoparticles do not have such overlapping redox potential and thus have a lower ROS induction potential (Zhang *et al.*, 2012). It is also known that CoO and La_2O_3 nanoparticles are insoluble at a neutral pH and will only dissolve in acidic conditions.

Analysis of the metal oxide suspensions of CoO and La_2O_3 nanoparticles revealed both particle systems differed in the hydrodynamic diameter when suspended in the cellular media used in this study.The CoO nanoparticle suspension was six times smaller than that of La_2O_3 nanoparticles; however, other parameters such as polydispersity, zeta potential and effective density were very similar across both suspensions. The difference in the agglomerate structure size consequently led to a drastic difference in the settling rate of the particles administered to the cells, with CoO nanoparticles depositing at a much lower rate than La_2O_3 nanoparticles For 90% of the administered dose of CoO and La_2O_3 nanoparticles to deposit, it would take an approximate of 43 and 3 h, respectively, in both experimental plates used in the study. Therefore, while the administered and cell delivered mass of La_2O_3 nanoparticles are equal, 85% of the administered CoO nanoparticles is the delivered mass after 3 h exposure. In spite of this lower delivered mass, CoO nanoparticles were more bioactive than La_2O_3 nanoparticles. When comparing the production of superoxide radicals with the multiple doses of CoO to La_2O_3 nanoparticles at both 6 and 24 h, the data suggest that CoO nanoparticles produce more ROS measured by DCFDA at both 25 and 50 μg/ml at both 6 and 24 h. These

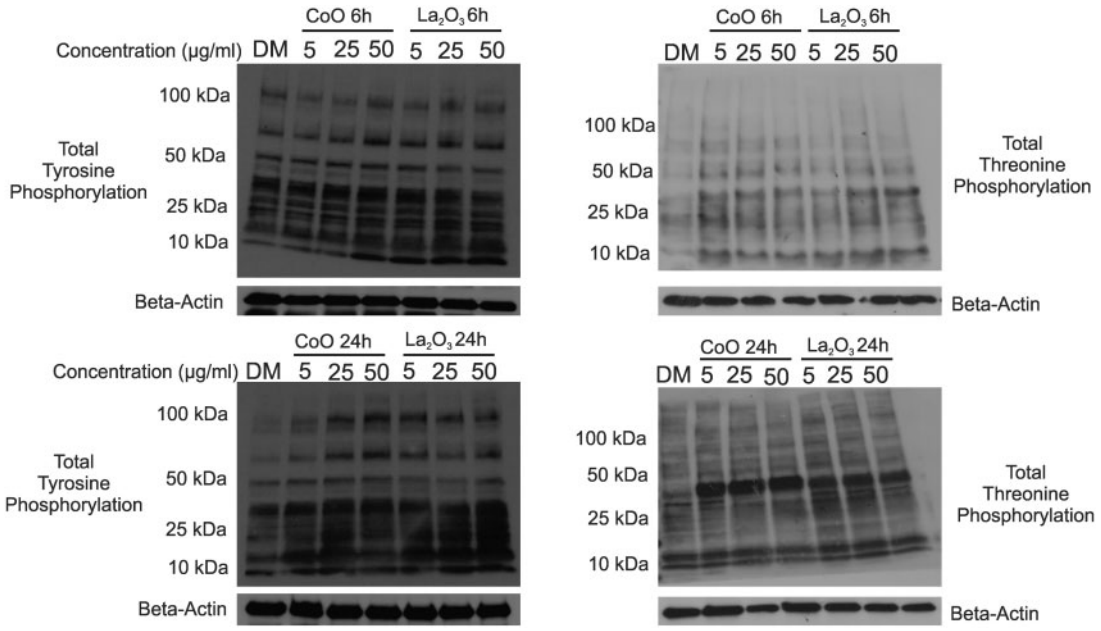

FIG. 5. Increase in total tyrosine and threonine phosphorylation. Whole cell lysates were collected from SAEC at both (A) 6 h and (B) 24 h treated with 0.0, 5.0, 25.0, or 50.0 μg/ml administered dose of CoO or La_2O_3 nanoparticles. Western blotting was used to detect changes in total tyrosine phosphorylation and total threonine phosphorylation. Beta Actin was used for internal control within the samples. Western blots are representative of n = 3.

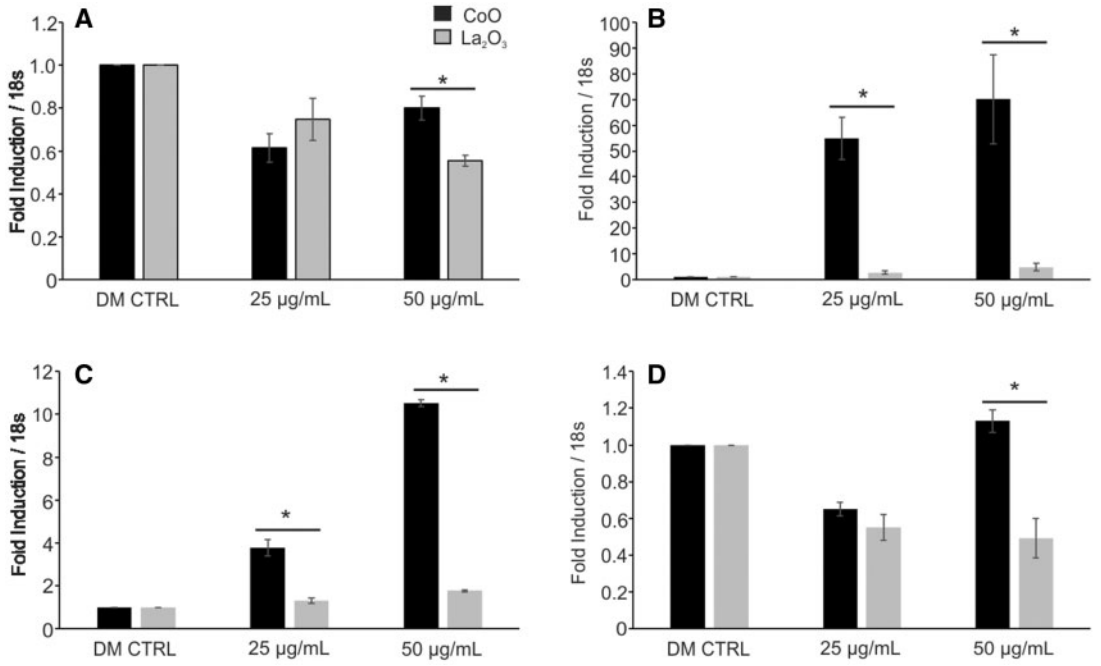

FIG. 6. Alteration in gene expression in SAEC due to CoO and La_2O_3 nanoparticles. cDNA generated from RNA was isolated from SAEC treated with 0.0, 5.0, 25.0, and 50.0 μg/ml administered dose for 6 h with CoO and La_2O_3 nanoparticles. cDNA was then assayed with TaqMan qRTPCR for the following genes: (A) NOS2, (B) MT3, (C) PTGS2(COX2), and (D) SOD3. Samples were normalized to internal control 18 s. The values represent a fold induction compared to 0.0 μg/ml control (1.0). n = 3, * indicates $P < .05$ compared to La_2O_3 nanoparticles at the same administered dose.

data correlate with the cytotoxicity MTS assay, which showed CoO nanoparticles were more toxic at both 25 and 50 μg/ml administered doses at both 6 and 24 h in comparison to La_2O_3 nanoparticles. ROS are a collective term for the intermediates formed during oxidative metabolism. Superoxide radicals (O_2^-) are a member of ROS, and the others include hydrogen peroxide (H_2O_2), hydroxyl radical (^-OH), and peroxynitrite ($ONOO^-$). All of these have been shown to induce cellular injury through DNA damage, protein oxidation, lipid peroxidation, cell growth, differentiation, and death alteration, as well as, cell signal transduction activation (Qian *et al.*, 2003). It has been demonstrated that nanoparticle-induced ROS production is related to alter molecular mechanisms that can lead to cytotoxicity, inflammation, fibrosis, and potentially tumorigenesis (Nel *et al.*, 2006). Several metal oxide nanoparticles have been demonstrated to induce cytotoxicity through the production of ROS production

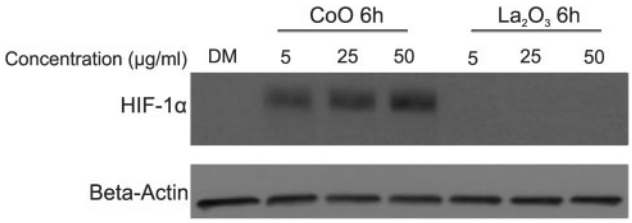

FIG. 7. Induction of HIF-1α due to CoO nanoparticles. Whole cell lysates were collected from SAEC at 6 h with 0.0, 5.0, 25.0, or 50.0 μg/ml administered dose of CoO or La_2O_3 nanoparticles. Western blotting was used to detect changes in HIF-1α protein expression. Beta Actin was used for internal control within the samples. Western blots are representative of n = 3.

(Nel *et al.*, 2006; Schrand *et al.*, 2010; Xie *et al.*, 2011). Taken together, this suggests that CoO nanoparticles produce more ROS leading to alterations in molecular pathways that lead to cytotoxicity. This could be due to an overlap of redox potential between CoO nanoparticles and ambient redox-active aqueous substances, leading to the electrons transferred between CoO nanoparticles and the cellular redox couples to induce ROS.

Tyrosine and threonine phosphorylation of proteins is the key step in activation of many cellular processes (Hunter, 1995; Marshall, 1995). In response to extracellular signals, protein phosphorylation occurs and leads to protein complex assembly and activation or inactivation of cellular signals (Pawson, 2004). It is well established that the changes in protein tyrosine and threonine phosphorylation play an essential role in cell proliferation, cell cycle progression, metabolic homeostasis, and transcriptional activation (Hunter, 1995; Macho *et al.*, 2015; Pawson, 2004; Schlessinger, 2014). The alteration of tyrosine/threonine phosphorylation is directly related to many human diseases, particularly cancer (Hunter, 1995). Changes in either tyrosine or threonine phosphorylation due to nanoparticle exposure can alter the cellular bioactivity on a global scale, as shown previously by our group (Mihalchik *et al.*, 2015). Our results suggest that there is a trend of larger global changes in both tyrosine and threonine phosphorylation in the CoO nanoparticle-treated cells in comparison to those treated with La_2O_3 nanoparticles. These data are significant because many molecular pathways activated by tyrosine and threonine phosphorylation play a role within cytotoxic pathways.

Induction of ROS within mammalian cells after exposure to nanomaterial tends to activate cellular antioxidant defenses, which can reduce oxidative stress in turn and induce the overexpression of many related genes. Moreover, ROS-induced DNA damage leads to gene expression alterations (Rahal *et al.*, 2014; Sarkar *et al.*, 2014; Xie *et al.*, 2011). After analyzing the profiles of gene expression following treatment of CoO or La_2O_3 nanoparticles, the data show that several genes related to oxidative stress (MT3, NOS2, PTGS2(Cox2), and SOD3) are elevated within cells treated with CoO nanoparticles at 6 h. MT3 is important in the cell for the removal of metals (Lee and Koh, 2010). NOS2 is needed for the synthesis of nitric oxide, which is a superoxide radical (Attia *et al.*, 2015; Colasanti and Suzuki, 2000). SOD3, superoxide dismutase, plays a key role in removing superoxide radicals within a cellular system where there is an over production of superoxide radicals (Fukai and Ushio-Fukai, 2011). PTGS2(Cox2) is a gene that is related to the antioxidant defense system within cellular oxidative stress (Luo *et al.*, 2011). These results suggest that CoO nanoparticles activate oxidative stress pathways within the SAEC when compared with SAEC dosed with La_2O_3 nanoparticles. However, since there is cytotoxicity seen in SAEC treated with La_2O_3 nanoparticles, it is possible that some cytotoxic pathways other than oxidative stress are playing a role in the bioactivity of La_2O_3 nanoparticles.

ROS production induces alteration in oxygen homeostasis which is regulated by a key transcription factor, HIF-1α (Kaewpila *et al.*, 2008; Wenger, 2000). Since ROS were induced by CoO nanoparticles within SAEC at 25 and 50 μg/ml at 6 h and there were altered gene expression related to oxidative stress at 6 h, HIF-1α protein expression was analyzed. Results showed HIF-1α protein expression was induced by CoO nanoparticles at all doses analyzed at 6 h, suggesting a HIF-1α dependent molecular mechanism is involved in CoO nanoparticle-induced cytotoxicity. Taken together, this study suggests that different toxicological modes of action are involved in CoO and La_2O_3 nanoparticle-induced toxicity in SAEC, which could be due to the difference of their physio-chemical properties, such as their band gap energy levels. CoO nanoparticles are more toxic than La_2O_3 nanoparticles in SAEC due to the activation of the different molecular signaling evidenced by the significant ROS production, tyrosine and threonine phosphorylation and gene expression observed in the cells post treatment, CoO nanoparticles also induce the protein expression of HIF-1α which could lead to a possible molecular mechanism for the CoO nanoparticle induced cytotoxicity in the SAEC that was not seen with the treatment of La_2O_3 nanoparticles. It will be of interest in the future to determine if CoO and La_2O_3 nanoparticle exposure in an *in vivo* experimental model leads to different profiles of inflammation and possibly lung fibrosis.

SUPPLEMENTARY DATA

Supplementary data are available online at http://toxsci.oxfordjournals.org/.

FUNDING

Funding from grants: NSF 1436450; NIH HL007118; NIH ES000002.

REFERENCES

Ametamey, S. M., Beer, H. F., Guenther, I., Antonini, A., Leenders, K. L., Waldmeier, P. C., and Schubiger, P. A. (1996). Radiosynthesis of [11C]brofaromine, a potential tracer for imaging monoamine oxidase A. *Nucl. Med. Biol.* **23**, 229–234.

Antonini, J. M., Krishna Murthy, G. G., Rogers, R. A., Albert, R., Ulrich, G. D., and Brain, J. D. (1996). Pneumotoxicity and pulmonary clearance of different welding fumes after intratracheal instillation in the rat. *Toxicol. Appl. Pharmacol.* **140**, 188–199.

Attia, M. S., Lass, E., and Loch Macdonald, R. (2015). Nitric oxide synthases: Three pieces to the puzzle? *Acta Neurochir. Suppl.* **120**, 131–135.

Burello, E., and Worth, A. P. (2011a). A theoretical framework for predicting the oxidative stress potential of oxide nanoparticles. *Nanotoxicology* **5**, 228–235.

Burello, E., and Worth, A. P. (2011b). QSAR modeling of nanomaterials. *Wiley Interdiscip. Rev. Nanomed. Nanobiotechnol.* **3**, 298–306.

Castranova, V. (2011). Overview of current toxicological knowledge of engineered nanoparticles. *J. Occup. Environ. Med.* **53**, S14–S17.

Chattopadhyay, S., Dash, S. K., Tripathy, S., Das, B., Mandal, D., Pramanik, P., and Roy, S. (2015). Toxicity of cobalt oxide nanoparticles to normal cells; an in vitro and in vivo study. *Chem. Biol. Interact.* **226**, 58–71.

Cohen, J., Deloid, G., Pyrgiotakis, G., and Demokritou, P. (2013). Interactions of engineered nanomaterials in physiological media and implications for in vitro dosimetry. *Nanotoxicology* **7**, 417–431.

Cohen, J. M., Derk, R., Wang, L., Godleski, J., Kobzik, L., Brain, J., and Demokritou, P. (2014a). Tracking translocation of industrially relevant engineered nanomaterials (ENMs) across alveolar epithelial monolayers in vitro. *Nanotoxicology* **8**(Suppl. 1), 216–225.

Cohen, J. M., Teeguarden, J. G., and Demokritou, P. (2014b). An integrated approach for the in vitro dosimetry of engineered nanomaterials. *Part Fibre Toxicol.* **11**, 20.

Colasanti, M., and Suzuki, H. (2000). The dual personality of NO. *Trends Pharmacol. Sci.* **21**, 249–252.

Deloid, G., Cohen, J. M., Darrah, T., Derk, R., Rojanasakul, L., Pyrgiotakis, G., Wohlleben, W., and Demokritou, P. (2014). Estimating the effective density of engineered nanomaterials for in vitro dosimetry. *Nat. Commun.* **5**, 3514.

Fukai, T., and Ushio-Fukai, M. (2011). Superoxide dismutases: Role in redox signaling, vascular function, and diseases. *Antioxid. Redox Signal* **15**, 1583–1606.

Hunter, T. (1995). Protein kinases and phosphatases: The yin and yang of protein phosphorylation and signaling. *Cell* **80**, 225–236.

Jeng, H. A., and Swanson, J. (2006). Toxicity of metal oxide nanoparticles in mammalian cells. *J. Environ. Sci. Health A Tox. Hazard Subst. Environ. Eng.* **41**, 2699–2711.

Kaewpila, S., Venkataraman, S., Buettner, G. R., and Oberley, L. W. (2008). Manganese superoxide dismutase modulates hypoxia-inducible factor-1 alpha induction via superoxide. *Cancer Res.* **68**, 2781–2788.

Katsnelson, B. A., Privalova, L. I., Sutunkova, M. P., Gurvich, V. B., Loginova, N. V., Minigalieva, I. A., Kireyeva, E. P., Shur, V. Y., Shishkina, E. V., Beikin, Y. B., *et al.* (2015). Some inferences from in vivo experiments with metal and metal oxide nanoparticles: The pulmonary phagocytosis response, subchronic systemic toxicity and genotoxicity, regulatory proposals, searching for bioprotectors (a self-overview). *Int J Nanomedicine* **10**, 3013–3029.

Kaweeteerawat, C., Ivask, A., Liu, R., Zhang, H., Chang, C. H., Low-Kam, C., Fischer, H., Ji, Z., Pokhrel, S., Cohen, Y., *et al.* (2015). Toxicity of metal oxide nanoparticles in *Escherichia coli* correlates with conduction band and hydration energies. *Environ. Sci. Technol.* **49**, 1105–1112.

Konduru, N. V., Murdaugh, K. M., Sotiriou, G. A., Donaghey, T. C., Demokritou, P., Brain, J. D., and Molina, R. M. (2014). Bioavailability, distribution and clearance of tracheally-instilled and gavaged uncoated or silica-coated zinc oxide nanoparticles. *Part Fibre Toxicol.* **11**, 44.

Lee, S. J., and Koh, J. Y. (2010). Roles of zinc and metallothionein-3 in oxidative stress-induced lysosomal dysfunction, cell death, and autophagy in neurons and astrocytes. *Mol. Brain* **3**, 30.

Lim, C. H. (2015). Toxicity of two different sized lanthanum oxides in cultured cells and Sprague-Dawley rats. *Toxicol. Res.* **31**, 181–189.

Littell, Ramon C, Stroup, Walter W, and Freund, Rudolf J. (2002). *SAS for Linear Models*, 4th ed. SAS Institute, Cary, NC.

Luo, C., Urgard, E., Vooder, T., and Metspalu, A. (2011). The role of COX-2 and Nrf2/ARE in anti-inflammation and antioxidative stress: Aging and anti-aging. *Med. Hypotheses* **77**, 174–178.

Macho, A. P., Lozano-Duran, R., and Zipfel, C. (2015). Importance of tyrosine phosphorylation in receptor kinase complexes. *Trends Plant Sci.* **20**, 269–272.

Marshall, C. J. (1995). Specificity of receptor tyrosine kinase signaling: Transient versus sustained extracellular signal-_regulated kinase activation. *Cell* **80**, 179–185.

Mcneilly, J. D., Heal, M. R., Beverland, I. J., Howe, A., Gibson, M. D., Hibbs, L. R,. Macnee, W., and Donaldson, K. (2004). Soluble transition metals cause the pro-inflammatory effects of welding fumes in vitro. *Toxicol. Appl. Pharmacol.* **196**, 95–107.

Mihalchik, A. L., Ding, W., Porter, D. W., Mcloughlin, C., Schwegler-Berry, D., Sisler, J. D., Stefaniak, A. B., Snyder-Talkington, B. N., Cruz-Silva, R., Terrones, M., *et al.* (2015). Effects of nitrogen-doped multi-walled carbon nanotubes compared to pristine multi-walled carbon nanotubes on human small airway epithelial cells. *Toxicology* **333**, 25–36.

Nel, A., Xia, T., Madler, L., and Li, N. (2006). Toxic potential of materials at the nanolevel. *Science* **311**, 622–627.

Oberdorster, G., Oberdorster, E., and Oberdorster, J. (2007). Concepts of nanoparticle dose metric and response metric. *Environ. Health Perspect.* **115**, A290.

Pal, A. K., Bello, D., Cohen, J., and Demokritou, P. (2015). Implications of in vitro dosimetry on toxicological ranking of low aspect ratio engineered nanomaterials. *Nanotoxicology*. **9**, 871–85.

Pawson, T. (2004). Specificity in signal transduction: From phosphotyrosine-SH2 domain interactions to complex cellular systems. *Cell* **116**, 191–203.

Piao, C. Q., Liu, L., Zhao, Y. L., Balajee, A. S., Suzuki, M., and Hei, T. K. (2005). Immortalization of human small airway epithelial cells by ectopic expression of telomerase. *Carcinogenesis* **26**, 725–731.

Qian, Y., Castranova, V., and Shi, X. (2003). New perspectives in arsenic-induced cell signal transduction. *J. Inorg. Biochem.* **96**, 271–278.

Rahal, A., Kumar, A., Singh, V., Yadav, B., Tiwari, R., Chakraborty, S., and Dhama, K. (2014). Oxidative stress, prooxidants, and antioxidants: The interplay. *Biomed. Res. Int.* **2014**, 761264.

Roy, R,. Kumar, S., Tripathi, A., Das, M., and Dwivedi, P. D. (2014). Interactive threats of nanoparticles to the biological system. *Immunol. Lett.* **158**, 79–87.

Sarkar, A., Ghosh, M., and Sil, P. C. (2014). Nanotoxicity: Oxidative stress mediated toxicity of metal and metal oxide nanoparticles. *J. Nanosci. Nanotechnol.* **14**, 730–743.

Schlessinger, J. (2014). Receptor tyrosine kinases: Legacy of the first two decades. *Cold Spring Harb. Perspect. Biol.* **6**, a008912.

Schrand, A. M., Rahman, M. F., Hussain, S. M., Schlager, J. J., Smith, D. A., and Syed, A. F. (2010). Metal-based nanoparticles and their toxicity assessment. *Wiley Interdiscip. Rev. Nanomed. Nanobiotechnol.* **2**, 544–568.

Verstraelen, S., Remy, S., Casals, E., De Boever, P., Witters, H., Gatti, A., Puntes, V., and Nelissen, I. (2014). Gene expression profiles reveal distinct immunological responses of cobalt and cerium dioxide nanoparticles in two in vitro lung epithelial cell models. *Toxicol. Lett.* **228**, 157–169.

Wenger, R. H. (2000). Mammalian oxygen sensing, signalling and gene regulation. *J. Exp. Biol.* **203**, 1253–1263.

Xie, Hong, Mason, Michael M., and Wise Sr, John Pierce. (2011). Genotoxicity of metal nanoparticles. *Rev. Environ. Health* **26**, 251–268.

Zhang, H., Ji, Z., Xia, T., Meng, H., Low-Kam, C., Liu, R., Pokhrel, S., Lin, S., Wang, X., Liao, Y. P., *et al.* (2012). Use of metal oxide nanoparticle band gap to develop a predictive paradigm for oxidative stress and acute pulmonary inflammation. *ACS Nano* **6**, 4349–4368.

Zhou, E. H., Watson, C., Pizzo, R., Cohen, J., Dang, Q., Ferreira de barros, P. M., Park, C. Y., Chen, C., Brain, J. D., Butler, J. P., *et al.* (2014). Assessing the impact of engineered nanoparticles on wound healing using a novel in vitro bioassay. *Nanomedicine* **9**, 2803–2815.